Open Research Online

The Open University's repository of research publications
and other research outputs

Nonlinear double-diffusive intrusions at the equator

Journal Item

For guidance on citations see FAQs.

Version: Accepted Manuscript

oro.open.ac.uk

Nonlinear double-diffusive intrusions at the equator

Neil R. Edwards[1] and Kelvin J. Richards[2]
1. Climate and Environmental Physics,
University of Bern, Switzerland.
2. IPRC/SOEST University of Hawaii,
Honolulu, Hawaii.

May 7, 2004

Abstract

Previous, linear analysis has suggested that observations of interleaving, quasi-horizontal layers in the equatorial oceans may be explained by double-diffusive or inertial instability. Here we describe an idealized, two-dimensional, numerical investigation of the nonlinear development of these instabilities, focusing almost exclusively on the double-diffusive case. We consider the mechanisms for equilibration and maintenance of the interleaving intrusions and perform a thorough sensitivity analysis. Nonlinearity arising from changes in diffusive regime is found to be more important than advective nonlinearity in promoting global equilibration. When variations in effective flux ratio are weak, local constraints prevent equilibration until large amplitudes are reached. When variations in flux ratio with density ratio are allowed, small-scale staircase and mesoscale intrusive instabilities coexist, leading to staircase-like intrusions with sharp, steppy interfaces. Solutions are found to equilibrate at between 3 and 13 times the amplitude where mean salinity gradients overturn. Cross-equatorial diffusivities between 20 and 400 m^2 s^{-1} are found in realistic cases with intrusion lengths of up to 40 km. A modified estimate of the effective cross-equatorial diffusivity based on a balance of lateral advection and vertical diffusion tends to overestimate the sensitivity to the mean horizontal and vertical gradients of salinity and underestimates the sensitivity to the vertical diffusivity but does give values within an order of magnitude of those derived from numerical experiments.

For comparison, we give a single example of inertially driven interleaving layers which reach 190 km in length giving cross-equatorial heat fluxes 4 times larger than realistic double-diffusively driven cases. Although the inertial case is not considered in detail, we speculate that observed interleaving is more likely to be created by inertial than double-diffusive instability.

1 Introduction

Observations of interleaving, quasi-horizontal layers with contrasting salinities and temperatures in the equatorial Pacific thermocline have been reported by several authors including Toole (1981), McPhaden (1985), Richards and Pollard (1991) and Richards and Banks (2002). Typically the layers are a few tens of metres thick and are found within a few degrees of the equator. The meridional extent of the intrusions is of the order of 100 km. Their extent in the zonal direction, along the equator, has been found to be in excess of 700 km (Lee and Richards 2004). The equatorial Pacific is characterized by strong mean northward thermohaline gradients as well as an active and complicated mean current system, including the equatorial undercurrent. Conditions are often favourable for microscale double-diffusive fingering, and mesoscale double-diffusive interleaving instabilities, of the type first described by Stern (1967), as well as inertial (or symmetric) instability, the theory of which goes back to Rayleigh (1916). Both of these mechanisms have been proposed as possible explanations of

1

observed equatorial processes, in particular Richards (1991) extended linear double-diffusive interleaving theory to the equatorial β-plane and Hua *et al.* (1997) proposed inertial instability as an explanation for deep equatorial jets, while Edwards and Richards (1999) developed a combined linear theory of double diffusive-inertial instability for the equatorial β-plane. Richards and Banks (2002), who consider an extensive set of measurements, find that the observed interleaving is consistent with both double-diffusive interleaving and inertial instability. Based on observations alone, they were unable to discriminate between the two mechanisms.

Here we strive to assess which of these mechanisms is likely to be dominant using a modelling approach. This requires that we model the nonlinear development of instabilities and attempt to estimate their likely amplitude in the fully-developed state. In the present paper we consider the double-diffusive mechanism in detail, modelling the growth and nonlinear equilibration of instabilties, and perform a thorough sensitivity analysis. We retain an idealized framework, considering only periodic, 2-dimensional disturbances to a background state with uniform mean gradients.

To model the nonlinear development of thermohaline intrusions it is necessary to use a parameterization of unresolved fluxes which appropriately handles stable and unstable stratifications which are not favourable to double diffusion, in addition to double diffusion-favourable stratification in both the fingering and diffusive regimes. The simplest option is to switch discontinuously between 4 different, constant diffusivities, depending on the background stratification. To avoid the awkward terminology "diffusive double-diffusive regime" we refer to the fingering and diffusive regimes by the relevant stabilizing vertical gradient, as "T-stable" or "S-stable" respectively.

In the one-dimensional case McDougall (1985) showed that steady-state interleaving states might exist if the flux ratio varied in the vertical, a situation which he assumed to be due to the coexistence of finger and diffusive interfaces. Following McDougall (1985), Walsh and Ruddick (1998) showed that the coexistence of finger and diffusive interfaces was necessary for equilibrium in their one-dimensional system, even though the effective flux ratio could vary within fingering or diffusive regions due to the linear combination of double-diffusive and turbulent fluxes. If the diffusivities are assumed to be separately constant within the T-stable and S-stable regions, then in the one-dimensional case, the change in diffusivity at the boundaries of different stability regions is the only source of nonlinearity. Hence there must be at least two regions for the system to behave in a nonlinear way, *a fortiori* there must be more than one type of region in any equilibrium solution. In two or more dimensions this is not necessarily true.

After presenting our model in the next section, we discuss the equilibration and maintenance of intrusions. We then attempt to determine what limits their growth and ultimately sets their amplitude, first comparing advective and diffusive nonlinearity (the latter normally a result of regime changes resulting from overturning of vertical gradients) then considering the generic effect of regime changes at opposing interfaces. We then perform a sensitivity analysis, relying on several simplifying concepts to identify the most fundamental independent parameters amongst the vast range of possible variables. Variations in diffusivity and flux ratio are also considered in a generalized and simplified sense, and the importance of both local and global constraints on equilibration investigated. In the final sections of the paper we consider the potential amplitude of double-diffusively driven interleaving for realistic parameters, using our earlier results to identify optimal parameters for maximal amplitude, and exhibit a single example simulation of an inertially unstable case for comparison. On the basis of our results, we speculate that double diffusion is unlikely to be the primary mechanism for the formation of the observed interleaving.

2   Governing equations and boundary conditions

Neglecting variations in the eastward, (x) direction, the two-dimensional flow (v, w) in a northward-vertical (y, z) plane can be represented by a streamfunction χ such that

$$v = -\frac{\partial \chi}{\partial z}, \quad w = \frac{\partial \chi}{\partial y}. \tag{1}$$

We make the β-plane assumption that the Coriolis parameter $f = \beta y$, but retain non-hydrostatic vertical acceleration. The governing equation for the zonal (x) component of vorticity, $\nabla^2 \chi$, is then taken to be

$$\frac{\partial}{\partial t} \nabla^2 \chi = -J(\chi, \nabla^2 \chi) + f \frac{\partial u}{\partial z} - \frac{g}{\rho_0} \frac{\partial \rho}{\partial y} + \nu_y \frac{\partial^2}{\partial y^2} \nabla^2 \chi + \nu_z \frac{\partial^2}{\partial z^2} \nabla^2 \chi - r \nabla^2 \chi, \tag{2}$$

where the Jacobian J represents advection associated with the streamfunction χ. The equations for zonal velocity u, temperature T and salinity S are

$$\frac{\partial u}{\partial t} = -J(\chi, u) - f \frac{\partial \chi}{\partial z} + \nu_y \frac{\partial^2}{\partial y^2} u + \nu_z \frac{\partial^2}{\partial z^2} u - ru, \tag{3}$$

$$\frac{\partial T}{\partial t} = -J(\chi, T) + \kappa_y \frac{\partial^2}{\partial y^2} T - r(T - \overline{T}) - \frac{\partial}{\partial z} F_T, \tag{4}$$

$$\frac{\partial S}{\partial t} = -J(\chi, S) + \kappa_y \frac{\partial^2}{\partial y^2} S - r(S - \overline{S}) - \frac{\partial}{\partial z} F_S, \tag{5}$$

and the equation of state is

$$\rho = \rho_0(\delta S - \alpha T), \tag{6}$$

where α and δ are the thermal expansion and saline contraction coefficients, which are assumed to be constant. An overbar denotes the background state and ρ_0 is a constant reference density. The y and z-components ν_y and ν_z of viscosity and the y-component of diffusvity κ_y are also assumed to be constant. We allow for a Rayleigh drag term with constant coefficient r following Hua *et al.* (1997) (our numerical code is a slightly modified version of the code used by these authors). Since r does not act preferentially on small scales it is best viewed as representing unresolved large-scale forces maintaining the initial, unstable state. The drag term is usually small, and its effect is discussed in Section 5(e). For runs with realistic parameters described in Section 6 we set $r = 0$ for ease of interpretation.

To parameterize the unresolved vertical fluxes of temperature and salinity F_T and F_S, we adopt a simplified form of the parameterization of Walsh and Ruddick (1998), as follows: fluxes F_Q, where $Q = T$ or S, will be deemed to have a contribution from double diffusion and shear-driven turbulence;

$$F_Q = D_Q + K_Q$$

where, in the T-stable, fingering regime $0 < \partial T/\partial z, 0 < \partial S/\partial z, \partial \rho/\partial z < 0$,

$$D_S = -A_F \frac{\partial S}{\partial z}, D_T = -\gamma_F \frac{\delta}{\alpha} A_F \frac{\partial S}{\partial z}. \tag{7}$$

In the S-stable regime, $\partial T/\partial z < 0, \partial S/\partial z < 0, \partial \rho/\partial z < 0$, the roles of T and S are reversed,

$$D_S = -\frac{\alpha}{\delta} A_D \frac{\partial T}{\partial z}, D_T = -\gamma_D A_D \frac{\partial T}{\partial z}. \tag{8}$$

Thus, in our notation, γ is always the ratio of heat to salt flux, $\gamma = \alpha D_T/(\delta D_S)$. If the fluid is fully stable $0 < \partial T/\partial z, \partial S/\partial z < 0, \partial \rho/\partial z < 0$, or statically unstable $0 < \partial \rho/\partial z$, then $D_S = D_T = 0$. The turbulent part is given by

$$K_S = -\kappa \frac{\partial S}{\partial z}, K_T = -\kappa \frac{\partial T}{\partial z}, \tag{9}$$

3

where the diffusivity $\kappa = \kappa_s$, for stable stratification and $\kappa = \kappa_u$, for unstable stratification. Default values of coefficients are given in Table 1. For the diffusive terms we follow Walsh and Ruddick (1998). The diffusivity of temperature in the S-stable regime ($\gamma_D A_D$ in our notation) is thus set equal to the salinity diffusivity A_F in the fingering regime unless stated otherwise. This may well overestimate A_D, a possibility which we consider in Section 4(b).

Solutions are assumed to be periodic in the vertical and to decay with distance away from the equator. The domain height is set to the vertical wavelength of the most unstable linear mode according to the theory of Edwards and Richards (1999). The background state is initially motionless, with linear variations of temperature and salinity in the vertical and meridional directions such that the density varies only in the vertical. Integrations are initialized by adding a small perturbation to the salinity field with the approximate form of the most unstable linear mode. We solve the equations numerically using a second-order finite difference method with, typically, 100 points in y and 40 points in z. Diffusion terms are lagged. To solve the Poisson equation for the streamfunction we use an exact semi-spectral method with a Fourier decomposition in the vertical direction.

3 Nonlinear equilibration

In order to perform a thorough sensitivity analysis we need to choose a set of default parameters for which steady solutions can readily be found in a sufficiently large neighbourhood. This is not a trivial problem, and we are forced to use default parameters which are somewhat different from those observed. This is perhaps inevitable, with foreknowledge of our ultimate conclusions. In Section 5 we rely on the understanding we have gained of the controlling mechanisms of interleaving to apply our results to more physically relevant parameter regimes. The parameters used and their default settings are given in Table 1. In this and the following sections we investigate the non-linear behaviour of double-diffusively driven intrusions. The parameter space is explored by varying those parameters which are found to be key to the development of the intrusions, and by eliminating certain physical processes in the equations. The details of the various experiments we report on here are given in Table 2 and the gross characteristics of the model solutions (cross-equatorial heat flux, intrusion length and amplitude) given in Table 3. We define the intrusion length l as the maximum lateral displacement of a contour of total salinity, see figure 1 for a schematic representation of interleaving structure and a graphical definition of l.

Using the default parameters of Table 1 the initial, exponential growth of the disturbance ultimately slows and a quasi-steady state is attained around 400 days into the simulation. Figure 2 shows the development of the maximum values of the zonal velocity and density perturbation during the simulation. Also plotted are the minimum values of vertical gradients of temperature and salinity and the maximum value of the vertical density gradient. Initially the vertical temperature and salinity gradients are everywhere positive, corresponding to the double-diffusive fingering-favourable (T-stable) background state. From the graph, salinity gradients overturn before temperature gradients, giving fully stable regions which persist in the final state, surrounding a region of double-diffusive convection in the diffusive or S-stable regime. In this run, which we will refer to as run S, no statically unstable regions develop. Perturbation fields of temperature, salinity, density, streamfunction and zonal velocity are shown in figure 3. Also shown is the total salinity field which remains dominated by the variation in the background state. The intrusion length is thus relatively small, while the large and uniform background gradients in our idealized scenario lead to unrealistically large variations across the domain.

Nonlinear equilibration is brought about by changes in the advection and vertical diffusion terms (the drag and horizontal diffusion terms also damp the instability, but these terms behave linearly, thus they can only affect the rate at which exponential growth occurs). Advection of the temperature and salinity perturbations by the vortical perturbation velocity leads to a rotation of the thermohaline fields, the sign of which is such as to flatten the fingering (T-stable) interface and steepen the diffusive (S-stable) interface. This advec-

tion pattern results in a reduction of the driving mean meridional thermohaline gradients in the centre of the disturbance and hence promotes equilibration. We later refer to this process as the advective equilibration mechanism.

At the S-stable interface where vertical gradients of temperature and salinity have reversed relative to the initial condition, double diffusion continues to smooth the temperature and salinity fields in the vertical, but the effect on density is opposite to that at the fingering interface, thus the S-stable interface exerts a braking effect on the instability, promoting equilibration. The effect is a reduction in the meridional density gradient and hence the zonal vorticity. This counteracts the advective tendency to steepen the interface, the gradient of which is roughly the same in the equilibrated solution as in the linear growth phase. Changes in diffusive regime thus act as sources of diffusive nonlinearity promoting equilibration. In the next Section we compare the relative importance of advective and diffusive nonlinearity in promoting equilibration. We regard both of these mechanisms as global constraints on equilibration since they allow the global structure of the flow to depart from the exponentially growing linear state. Later, in Section 5(e) we discuss a further constraint on equilibration which is local in origin. Our distinction between local and global thus refers to the origin of the mathematical constraint, rather than to any distinction of physical processes or timescales. For a global equilibrium solution, both types of constraint must be satisfied.

We define an effective cross-equatorial diffusivity of heat κ_{eff} as the average advective heat flux across the equator divided by the mean thermal gradient specified in the initial condition. In the final state of run S the effective diffusivity is 107 m^2 s^{-1}.

Examination of the energy budget for the disturbance shows that the steady-state interleaving in this default solution is artificially sustained by the periodic boundary conditions in the vertical. However, very similar solutions are obtained in vertically much larger domains where the influence of the boundaries on the layers in the centre of the domain is small (run XPF in Table 2. In such cases a quasi-steady state can be maintained for at least 5 years (our longest simulation) by a steady reduction in the potential energy of the background state. Mean vertical gradients of T and S steadily reduce in these simulations, and there is a slow decrease in wavenumber of around 5% per year.

4   Amplitude of nonlinear intrusions

a. Advective versus diffusive nonlinearity. Because the amplitude of the steady-state interleaving ultimately determines the magnitude of the resulting effect on the large-scale flow, it is essential to understand what sets this amplitude. As discussed in Section 3, either advection or diffusion could provide the global source of nonlinearity (the latter via regime changes) required to limit exponential growth and promote equilibration. Changes in flux ratios, as discussed by Walsh and Ruddick (1998), provide a further constraint on equilbriation which is local in origin. We discuss this local constraint in Section 5(e).

The relative importance of advective and diffusive nonlinearity can be addressed by suppressing various terms in the governing equations. When all advective nonlinearity is suppressed (run D), the resulting steady state is of similar amplitude to run S. In contrast, when advective nonlinearity is retained, but diffusive regime changes are suppressed (run A), a steady state around 4.5 times larger is obtained, with an effective diffusivity of 1200 m^2 s^{-1} and intrusive features of length around 80 km clearly visible in the total salinity field. It turns out that even in this latter run it is the overturning of the vertical density field which controls the amplitude of the final solution via nonhydrostatic effects. The salinity gradient overturns in the linear solution when the perturbation salinity gradient, with amplitude mS', equals the mean gradient $\Delta S/H$, where $m = 2\pi/H$ is the vertical wavenumber. Thus if we define a dimensionless disturbance amplitude $a = 2\pi S'/\Delta S$ then a is the ratio of the salinity perturbation amplitude to the amplitude at overturning. Peak values of a are given in Table 3. For runs S and D, a reaches about 3, while in run A, a reaches 14. When nonhydrostatic effects and diffusive regime changes are removed (run AH), so that the system

5

has no knowledge of the background gradients, oscillatory solutions are obtained in which advective nonlinearity leads to a complete removal of the driving thermohaline gradients, which are then slowly reestablished by drag or diffusion terms. Advective nonlinearity is thus sufficient to cause equilibration, eventually limiting the dimensionless amplitude to around 20, but diffusive regime changes control the steady-state amplitude unless unphysical diffusive parameters are specified.

b. The limit of weak braking at the opposite interface. The full specification of the diffusivity in each of the different diffusive regimes involves a large number of parameters, but the above results suggest that we may make progress by considering an important limiting case. The symmetry of the double-diffusive flux parameterisations implies that the formation of the opposing double-diffusive interface (here the S-stable regime) after the overturning of the mean gradients always exerts a braking effect on the growth of the instability. We can define a limiting case of weak braking at the opposite interface either by setting the flux ratio γ_D in the S-stable regime to 1, corresponding to normal diffusion with vanishing double-diffusive interleaving growth rate, or by removing double-diffusive fluxes altogether at that interface, setting $A_D = 0$. It turns out that the latter case (run WB in Tables 2 and 3) is more interesting, equilibrating at more than double the dimensionless amplitude of the standard run S with more than 4 times the (quadratic) cross-equatorial heat flux and much greater intrusion length (an intermediate result is obtained by simply setting $\gamma_D = 1$). The equilibration of run WB is qualitatively similar to the standard run S, although much more negative vertical gradients of T and S are achieved, since with $A_D = 0$ the system is unable to extract the potential energy of the unstable temperature gradient. $\partial T/\partial z$ and $\partial S/\partial z$ reach -0.115 K/m and -0.13 psu/m respectively in run WB as against -0.012 K/m and -0.052 psu/m in run S. However, the total density still does not quite overturn in run WB, although the density gradient reaches -0.0025 kg/m^4, a quarter of the maximum value in run S.

The braking effect of the opposite interface in our standard case therefore has a significant limiting effect on the final amplitude of the interleaving. However, the weak-braking result is conceptually useful in providing an upper bound on the possible amplitude of solutions for any form of double diffusive flux parameterisation in the S-stable regime. Although weak braking results in much greater amplitude, $a = 8.4$ in run WB while $a = 3.1$ for run S, this is still significantly smaller than the value of $a = 21$ found in run AH with no diffusive nonlinearity at all. Thus even for arbitrarily weak double-diffusive braking at the opposite interface the steady-state amplitude is still strongly controlled by the nonlinear diffusive effect of the change in our flux parameterisation between the remaining stability regimes. In view of these results we can obtain at least order-of-magnitude bounds on the possible amplitude of equilibrated layering instabilities by varying only the behaviour at the dominant interface, in particular, the influence of the initial values of mean gradients and hence the amplitude of the instability at the point at which they overturn.

5   Parameter sensitivity

To understand the sensitivity of the intrusion amplitude to the wide variety of parameters involved, it is helpful to clarify the problem somewhat. In principle, we need to consider the effect of all the independent parameters which affect amplitude. The amplitude is governed by nonlinear processes, since the linear problem leads only to exponential growth or decay. Thus we can ignore, at least initially, the small parameters ν_y and r representing lateral diffusion and Rayleigh drag. These affect the linear growth and may have an effect at very long timescales, but since they act linearly, they are unlikely to significantly affect the amplitude at which the intrusions first equilibrate (the turbulent diffusivity κ_s, although linear, has a potentially greater effect for reasons discussed later).

Analysis of the linear problem reveals that it depends on only 4 dimensionless parameters;

the thermohaline gradients in the horizontal and vertical directions, the Schmidt number $\sigma = \nu/A$ and a number representing the relative effects of rotation and vertical diffusivity given by

$$s = \frac{\beta^2 A}{N^3}.$$

The buoyancy frequency N simply sets the overall timescale for the problem and is not independent of the other parameters. We continue to present our results in dimensional form, but restrict ourselves henceforth to a consideration of the independent parameters σ and diffusivity A (in lieu of s), in addition to the effects of the mean thermohaline gradients and the form of the double-diffusive fluxes. With N fixed, variations in vertical salinity gradient are equivalent to variations in the density ratio $R_\rho = (\alpha \partial T/\partial z)/(\delta \partial S/\partial z)$.

a. Background gradients. The results of the previous sections suggest that an increase in the vertical salinity gradient should result in larger fluxes assuming that the equilibrium dimensionless amplitude is roughly unchanged. This is indeed the case, as can be seen from the results of run SZ in Table 3. Since we maintain a constant value for the vertical density gradient, doubling the salinity gradient leads to a smaller increase, by a factor around 1.4, in the temperature gradient. The dimensionless amplitude is somewhat smaller, 2.3 as against 3.1 in run S, the maximum density perturbation being 1.5 times larger and the (quadratic) heat flux being 2.4 times larger. However, the intrusion length is still small, around 30 km. Note that increasing $\partial S/\partial z$ amounts to reducing the initial density ratio R_0. $R_0 = 1.89$ in run SZ as compared to 2.78 in run S.

Doubling the lateral salinity gradient increases the dimensionless amplitude to 5.2 and increases the heat flux and density perturbation but results in smaller effective diffusivity κ_{eff} and intrusion length l, see run SY in Table 3. This run equilibrated in two stages and has a slightly more complex spatial structure in the steady state (not shown).

b. Prandtl/Schmidt number. Linear analytical solutions found by Richards (1991) show that the initial growth rate of double-diffusive intrusions is proportional to $\sigma^{-1/2}$, while the most unstable vertical wavelength is proportional to $\sigma^{1/2}$. The amplitude of our nonlinear steady-state solutions is also dependent on σ. In relation to run S, doubling σ is found to increase the maximum density perturbation by a factor of 1.17 (run 2S), and to increase the heat flux by a factor of 1.09. Increasing σ by a factor of 10, however, gives only a 41% increase in maximum density perturbation and a 10% increase in heat flux.

Thus although increasing σ reduces the growth rate in the linear phase, larger values of σ ultimately result in larger steady states. For a given amplitude a the amplitude of the salinity perturbation will be directly proportional to the wavelength. This suggests that the density perturbation amplitude should also be roughly proportional to the wavelength. Doubling σ increases the vertical wavelength by 15% while increasing σ by a factor of 10 leads to a 77% increase. Thus the increase in density perturbation amplitude is largely explained by the change in vertical wavelength although the heat flux, which would be expected to be quadratic in the disturbance amplitude, increases less than the density perturbation in this case. On the other hand the intrusion length increases to 35 km when σ increases by a factor of 10 while the amplitude a remains close to 3. This increase is probably due to the increase in horizontal scale of the linear (and nonlinear) solution.

c. Diffusivity/rotation number. For the reasons discussed above we restrict our consideration of the diffusivity to the dominant, T-stable (fingering) regime. As noted earlier, this amounts to changing the relative effects of rotation and diffusion. To separate the effects of changing diffusivity A (or s) and σ, we keep the latter constant. As a first step we consider variations in the value of A when it is assumed to be spatially constant. On simple dimensional grounds, in the absence of a dependence on the relevant dimensionless parameter s, increasing A

should have no effect on the density perturbation while the increase in the heat flux should be proportional to $A^{1/2}$. In fact, increasing A by a factor of 2 or 4 gives an even greater increase in the density perturbation (see Table 3) and the heat flux increases by a factor of 3.2 or 12.6 respectively. These substantial increases can only partly be explained by the effect of A on the vertical wavelength, which increases by 15 and 47% respectively in the two runs.

d. Variable diffusivity. Our greatest uncertainty concerns the true form of the double-diffusive fluxes. Restricting our consideration (as above) to the dominant, T-stable (fingering) regime we perform a limited investigation of the possible effect of variation of the fingering diffusivity A with the mean gradient, but we further restrict our attention to qualitative variations of A with the density ratio R_ρ. The use of eddy diffusivities which vary with the mean gradient can lead to Phillips-Posmentier type layering instabilities (Posmentier 1977, Balmforth *et al.* 1998, Walsh and Ruddick 1995b). To avoid the theoretical possibility of arbitrarily large growth rates at vanishingly small vertical scales, we specify a diffusivity which varies between two constant values over a finite region. This ensures that any layering instabilities should at least have a finite maximum steepness. The extent of uncertainty as to the true variation of A with R_ρ is such that formulations have been proposed which differ even with regard to the sign of this variation. Schmitt (1981) proposing a decrease with R_ρ and Kunze (1987, 1994) proposing an increase. In the context of this uncertainty, we simply compare the effects of specifying formulations for A which increase, or decrease, at varying rates.

Diffusivity is thus assumed constant everywhere except between two finite limits, R_1 and R_2, of R_ρ in the T-stable (fingering) regime. We start with the case in which $R_1 < R_2 < R_0$ in order to avoid modifications to the linear problem (Walsh and Ruddick 1995b). We also keep constant the turbulent diffusivity κ and the Schmidt number σ, which for the runs in this section is defined as $\sigma = \nu/(A_F + \kappa_s)$ in the T-stable (fingering) regime and $\sigma = \nu/(A_D + \kappa_s)$ in the S-stable regime.

The diffusivity in T-stable regions is thus defined by

$$
\begin{aligned}
A &= A_1 : R_\rho \le R_1, \\
A &= A_1 + 0.5(A_2 - A_1)(1 - \cos(\pi \frac{R_\rho - R_1}{R_2 - R_1})) : R_1 < R_\rho < R_2, \\
A &= A_2 : R_\rho \ge R_2.
\end{aligned}
\tag{10}
$$

At the fingering-favourable interface in run S, R_ρ decreases from its initial value of 2.78 and attains a minimum value of 1.9 (at the opposite interface R_ρ increases and changes sign at infinity as the mean gradients overturn). To encompass this range of nonlinear variation in R_ρ we set $R_1 = 1.5$ and $R_2 = 2.5$. A_2 is set to the value A_0 used in run S to give the same initial linear problem and we consider the 4 cases in which A either increases or decreases by a factor of 2 or 5 between A_1 and A_2. We refer to these runs as D+2, D+5, D-2 and D-5 respectively (see Table 4).

The variation of diffusivity in run D+2 is qualitatively as expected. The density ratio R_ρ decreases to a minimum value in the centre of the fingering region, as in run S, and the diffusivity decreases smoothly to a minimum there. In run D-2 the variation of A is somewhat more complicated, as shown in figure 4. The diffusivity is larger than its background value throughout the fingering region, evidencing a reduction in R_ρ, but the centre of the fingering region is a vertical minimum of diffusivity, which increases away from the fingering interface towards a maximum in the convective regions which surround the S-stable interface. Thus the vertical variation of R_ρ in this run has reversed, with R_ρ maximal at the centre of the fingering region. Both signs of variation of A therefore lead to a minimum of A at the fingering interface and neither leads to a sharpening of the interfaces. The increased gradient of the change in A in runs D+5 and D-5 does not change this result. It is therefore not surprising that the spatial variation of A in these runs does not produce larger amplitude

8

interleaving. The two runs D+2 and D+5 in which A increases with R_ρ result in steady states smaller than run S. In runs D+2 and D+5 the diffusivity A decreases with R_ρ from a maximum value which is 2 or 5 times larger than the standard value respectively. Although these runs produce larger steady states than run S, as detailed in Table 3, the amplitudes of fluxes and the length of the intrusions are smaller than in the run with constant diffusivity equal to twice the standard value, run D2. Relaxing the constraint that A be constant in the linear regime and repeating the above set of runs leads to solutions of similar or smaller amplitude. There is no evidence from any of the runs described in this section that variation of A with R_ρ, in the absence of other changes, is likely to lead to strong changes in the equilibrated amplitude of nonlinear intrusions.

e. Turbulent diffusivity and flux ratio. Although the additional turbulent diffusion is a linear term and is therefore incapable of bringing about global equilibration of the intrusions, it is a prerequisite for local equilibrium and hence for the existence of steady solutions in the one-dimensional case considered by Walsh and Ruddick (1998). This is because in one dimension the ratio of temperature and salinity advection is fixed by the constancy of gradients along the layers, while the ratio of temperature and salinity diffusion is fixed if the diffusive flux ratio is a constant. These constant ratios will generally be different and thus simultaneous equilibrium of both T and S is impossible unless the ratio of diffusive fluxes is allowed to vary. Variations of the flux ratio γ are known to be important (see below) but even with γ set to a constant for simplicity, the inclusion of turbulent diffusivity κ_s allows the effective flux ratio, γ_{eff} (the ratio of total diffusive fluxes of T and S) to vary (Walsh and Ruddick 1998) and thus removes the obstruction to equilibration. In two dimensions the ratio of advective terms need not be constant; in the nonlinear phase the temperature, salinity and streamfunction perturbations in our solutions all have slightly different spatial structures, thus it is not obvious whether or not steady solutions are theoretically possible with constant effective flux ratio in two dimensions, although strong constraints exist, for instance the density ratio R_ρ must equal γ throughout any fingering region enclosed by a single streamline. Given our parameterisation with constant γ, the value of the turbulent diffusivity κ_s may therefore have a significant effect on steady solutions, even if it is not essential for their very existence. If variations in both the advective flux ratio and γ_{eff} are weak then local equilibration may not occur until the solution reaches large amplitude. Note that this form of local control on the amplitude of solutions is quite separate from the global requirement of a source of nonlinearity to restrict the initially exponential growth.

In run S, κ_s has the relatively large value of 10^{-5} m^2 s^{-1}, or one third of A_0. When κ_s is halved (run K/2) a smooth steady state obtains which is qualitatively similar to run S except that convective regions exist in the steady state and the amplitude is around 25% larger. Referring to Table 3, the sensitivity to κ_s is thus not particularly strong compared to the diffusivity A or the thermohaline gradients. However, if κ_s is reduced by a factor of 10 or set to zero, the behaviour is rather different. Although solutions equilibrate, the fluid becomes statically unstable almost everywhere outside of a sharp density jump at the fingering interface, and a smaller jump at the opposite interface. Although such density jumps are not resolved by the code, a repeat run with $\kappa_s = 0$ with 4 times the vertical resolution gave fluxes differing by only 4%, indicating weak sensitivity to the unresolved layer thickness. In our system we allow for two further dissipative parameters in the T and S equations (4) and (5); a horizontal diffusivity κ_y and a Rayleigh drag r. Setting $\kappa_s = r = \kappa_y = 0$ (run T0 in Tables 2 and 3) leads to a solution of considerably larger amplitude than the $\kappa_s = 0$ case (for which we obtain $a = 3.3$) even though convection is almost ubiquitous for small, non-zero κ_s, κ_y and r. Indeed the dimensionless amplitude of run T0, $a = 13$, is similar to that in run A, where $a = 14$, although the fluxes and intrusion lengths remain smaller. Time series of relevant quantities during the equilibration of run T0 are shown in figure 5.

These small diffusive parameters therefore have a powerful effect on the solution amplitude even well beyond the point where convection strongly modifies the effective diffusive

9

flux ratio throughout the solution. In run A only advective and convective effects can promote the global nonlinearity required for equilibration, whereas in run T0 advection and convection are the only sources of variation in the flux ratios required for local equilibration. Local and global constraints on equilibration thus appear to be of roughly comparable importance.

Variations of the flux ratio γ itself may be dynamically important. In direct numerical simulations of double-diffusive fingering conducted by Radko (2003), the decrease of γ with density ratio R_ρ is shown to be responsible for the spontaneous formation of a system of convective layers separated by fingering regions, a so-called thermohaline staircase, in the numerical simulations. Various functional forms for $\gamma(R_\rho)$ have been proposed, see Walsh and Ruddick (2000) and references therein, sharing the general property that the flux ratio decreases from a value less than or equal to 1 at $R_\rho = 1$ to a value around 0.5 at $R_\rho \approx 4$. Beyond this point the formulations diverge, but it is the lower values of R_ρ that are most important here. Walsh and Ruddick (2000, see also Radko 2003) show that the decrease of γ can lead to a layering instability for R_ρ sufficiently close to 1 and for small values of additional turbulent diffusivites. We have performed a limited investigation of the effect of such variations on our solutions using the form derived analytically from salt-finger linear instablity theory by Stern (1975),

$$\gamma_{\mathrm{F}} = R_\rho - \sqrt{R_\rho(R_\rho - 1)}. \tag{11}$$

The effect of using this parameterisation in our standard run is very small. This is not surprising, since the range of R_ρ in run S, from 1.9 to 2.8, corresponds to a very small range of variation of $\gamma_F(R_\rho)$ from 0.56 to 0.59. Quantitative changes are slightly larger for smaller initial values of R_ρ, cf run SZ, but qualitatively different behaviour, as compared with constant γ, was found when the turbulent diffusivity κ_s was set to zero. In this run, GR in Tables 2 and 3, variations in flux ratio γ cannot be dominated by variations in effective diffusive flux ratio due to κ_s and a two-stage instability process occurs. Small-scale instability appears first at grid scale, with vertical layers merging to give a system of vertically alternating finger and convection layers, randomly distributed throughout the domain, around 100 km in lateral extent and around 2.5 m high. This staircase structure does not appear to inhibit the interleaving instability, although lateral fluxes due to interleaving are initially suppressed. As the interleaving develops, the convecting layers in the interleaving region merge to leave a single convecting layer and a single, steppy, fingering interface in the (vertically periodic) domain. In the final state, cross-equatorial interleaving fluxes are 4 times as large as in the standard run S and twice as large as those obtained simply by setting $\kappa_s = 0$ without modifying γ. A thorough investigation of such a complex flow, with two separate scales of instability, is beyond the scope of this study, however, we note that simply doubling the vertical resolution gave very similar results for the final interleaving amplitude and for the vertical scale of the staircase throughout most of the run, although the staircase developed more rapidly in the initial stages. Although we lack the resources to study this situation thoroughly, our limited investigation supports the suggestion that variations in γ can lead to the formation of thermohaline staircases, which merge into steppy interfaces in the presence of mesoscale interleaving instability, possibly enhancing the lateral fluxes due to the interleaving. The temperature perturbation in run GR is shown in figure 6 after the development of the staircase structure and in the final state of fully developed interleaving.

6 Interleaving at more realistic parameters

The above results represent a fairly thorough, but essentially idealized, sensitivity study of the amplitude of steady-state double-diffusively driven equatorial interleaving. In order to carry out the sensitivity analysis, we were forced to choose a default case at a convenient position in parameter space, where stable solutions could readily be found in a reasonably large neighbourhood. These default parameters are rather different from the observational

estimates of Richards and Banks (2002) corresponding to periods when interleaving was observed. These authors estimate $N^2 = 1.7 \times 10^{-4}$ s^{-1}, and mean salinity gradients $\overline{S}_y = 1.7 \times 10^{-6}$ psu m^{-1} and $\overline{S}_z = 0.002$ psu m^{-1}. A widely quoted estimate for the fingering diffusivity calculated from observations of meddy Sharon is $A_F = 3 \times 10^{-5}$ m^2 s^{-1} (Ruddick and Hebert 1988) but Walsh and Carmack (2003) obtain a much smaller value of 0.8×10^{-5} m^2 s^{-1} from the large-scale spreading of Atlantic water in the Arctic. Ledwell (personal communication) finds values as large as 8 to 9×10^{-5} m^2 s^{-1} east of Barbados but only 1.7×10^{-5} m^2 s^{-1} in the subtropical gyre. To cover this range of estimates, we perform nonlinear simulations at both 1 and 10×10^{-5} m^2 s^{-1}, taking the lower of the two as a default for the linear growth rate calculations, which are almost independent of A.

At these "best guess" parameters there is no double-diffusive interleaving solution as the flow is not even linearly unstable. Indeed, the potential for finding nonlinear, finite amplitude solutions at nearby parameter values is essentially restricted by the existence of linear instability, rather than any difficulties or features of the nonlinear equilibration. To illustrate the range of parameters at which linear instability occurs in our 2-D system, we use the linear solution of Edwards and Richards (1999) to plot in figure 7 the value of lateral salinity gradient $\overline{S}_y$ at which the linear growth rate of double-diffusive interleaving equals 10^{-7} s^{-1}, corresponding to an e-folding time of around three months, as a function of N^2 and $\overline{S}_z$. For this figure we used the values $A = \nu = 10^{-5}$ m^2 s^{-1}, $\kappa_s = 10^{-6}$ m^2 s^{-1}, $r = 0$. Linear growth rates are insensitive to A, relatively insensitive to $\overline{S}_z$ but more strongly, and monotonically, dependent on $\overline{S}_y$ and N^2.

Given the uncertainty concerning parameterizations and parameter values, and the possibility that observed gradients may correspond to equilibrated, rather than unstable, mean values, the absence of instability at observed mean gradients may not rule out double diffusion as a formation mechanism for the intrusions. We therefore use the figure to identify a set of unstable mean gradients "close" to those observed and compute further nonlinear integrations at these near-observed values. Note, however, that to obtain reasonable, positive linear growth rates we use an initial lateral salinity gradient 3 times larger than the observational estimate and a vertical density gradient 3 times smaller. The relevant runs are denoted OBS1, OBS2 and OBS3 in Table 3 where the parameters used are listed. Qualitatively the equilibration of these runs is similar to those described earlier, although convective regions are present in the solution, in addition to the 3 statically stable regimes, while in OBS2 and OBS3 the zonal velocity does not fully equilibrate, drifting slowly throughout the integration. With default values for diffusivities of $A = \nu = 10^{-5}$ m^2 s^{-1}, $\kappa_s = 10^{-6}$ m^2 s^{-1}, $r = 0$ in run OBS1, fluxes and effective diffusivity κ_{eff} are small, indeed, for this run $\kappa_{\text{eff}} = 19$ m^2 s^{-1} (see Table 4). However, the strong dependence of equilibrated interleaving fluxes on sub-grid scale diffusivities is evident from run OBS2 in which the diffusivity A is increased by a factor of 10 to 10^{-4} m^2 s^{-1}, at the upper limit of plausible values discussed above. This leads to a more than 8-fold increase in effective lateral diffusivity. Finally, in run OBS3, we rely on our earlier results to suggest the diffusivity parameters which should produce the largest possible interleaving structure at plausible parameters. For this run, therefore, we retain the very high value of fingering diffusivity A_F, but use a very low value for the diffusivity A_D at the opposing interface of 10^{-5} m^2 s^{-1}, to give "weak braking". As in OBS1 and OBS2, the turbulence parameters are also kept small. In this "optimal double diffusion" run, we finally manage to obtain a significant intrusion length of 42 km, along with an effective diffusivity around 400 m^2 s^{-1}. The total salinity field in the steady state is shown in figure 8.

7 An example inertially unstable case

We conclude with a single example case which is unstable to inertial instability. This experiment is denoted II in Table 2. Parameters are as far as possible the same as those of runs OBS1 to OBS3; the parameters closest to observational estimates which permit double-diffusive instability. To drive inertial instability we impose, in addition, a lateral shear of

amplitude 4×10^{-6} s^{-1}, a reasonable value for equatorial mean flows. The temporal development of the instability is shown in figure 9. The instability grows to large amplitude and eventually removes the driving unstable gradient of angular momentum. Cross-equatorial heat and salt fluxes are caused by essentially passive advection of mean thermohaline gradients and are four times larger than those found in realistic double-diffusively driven runs. Intrusive thermohaline features develop and grow to lengths of hundreds of km, as shown in figure 10, before vertical mixing by secondary instabilities, possibly due to shear, obscures this vertical structure.

8   Discussion and conclusions

The nonlinear development and equilibration of double-diffusive intrusions at the equator has been modelled in an idealized, two-dimensional framework. Finite amplitude, quasi-steady layering solutions exist which can be sustained for long periods by a transfer of potential energy from the background state. In our standard solution the dimensionless amplitude a, the amplitude of the salinity perturbation relative to the amplitude when the mean salinity gradient overturns, reaches a value around 3 in the final state. Although advective nonlinearity would ultimately limit the amplitude of the intrusions to a value $a \approx 20$, the controlling factor in all cases studied (except for those with artificial suppression of regime changes) is the braking effect created by the appearance of the opposing double-diffusive interface when the mean vertical gradients overturn. The opposing interface has a braking effect as long as the flux ratio is greater than one in S-stable (diffusive) double diffusion and less than one in T-stable (fingering) double diffusion, which it must be if the microscale fluxes are driven by the release of background potential energy.

The existence of both T- and S-stable double-diffusive regimes vastly increases the potential complexity of the sensitivity analysis. To avoid excess complication we treat the effect of the opposing interface by considering a single limiting case, that of an arbitrarily weak double-diffusive effect there. The amplitude in this case reaches 8 times the overturning amplitude. Thus the braking effect in our standard run is important, but even with arbitrarily weak double-diffusive fluxes at the opposite interface, the change in diffusive regime provides a stronger constraint on intrusion growth than advective effects.

Equilibrated dimensionless amplitudes were found to increase weakly with Prandtl / Schmidt number and strongly with the basic value of the fingering diffusivity. Amplitude a increases with mean lateral salinity gradient and decreases with vertical salinity gradient but the change in cross-equatorial diffusivity κ_{eff} is opposite. An investigation of the qualitative effect of variations in diffusivity with density ratio showed no evidence that variable diffusivity in itself could lead to much larger amplitude solutions.

When turbulent diffusivity κ_s is small compared to fingering diffusivity A_F, weak variations in effective flux ratio γ_{eff} (Walsh and Ruddick 2000) provide a local constraint which prevents equilibration until large amplitudes are reached, in some simulations up to 13 times the overturning amplitude. Local and global constraints on equilibration thus appear to be of roughly comparable importance. In such cases the solution is statically unstable everywhere outside of a thin fingering interface. For such small turbulent diffusivities it becomes appropriate to allow for variation of the flux ratio γ itself (as opposed to γ_{eff}). Using the functional dependence suggested for $\gamma(R_\rho)$ by Stern (1975) we find, in one example case, that small-scale thermohaline staircase structures develop early in the simulation. This supports Radko's (2003) numerical result that thermohaline staircases can develop purely as a result of the decrease of flux ratio γ with R_ρ. This process has also been thoroughly investigated in the laboratory by Krishnamurti (2003). Staircase formation in our case does not appear to inhibit the formation of mesoscale interleaving structures which reach an amplitude around $a = 5$. Within the intrusion region, convective layers merge to fill the periodic domain, leaving only a single, steppy fingering interface in each intrusion layer. Staircase and mesoscale intrusion formation instabilities can therefore coexist, and doubtless interact, in our simulations leading to intrusions which are also staircases (that is, vertically alternating finger and

convecting layers). This supports Merryfield's (2000) suggestions for staircase formation via interleaving. Thus in our simulations the vertical extent of the convective region, compared to the vertical intrusion wavelength, varies from zero in the standard case to almost one. Staircase formation is favoured by smaller background R_ρ, so that density overturns soon after salinity, as in run SZ, and in large amplitude states, in particular for weak turbulent diffusivity.

Whether these results remain qualitatively true away from the equator remains a matter of conjecture, since our numerical method, and the dynamical trapping of interleaving structures close to the equator, makes it non-trivial to apply our results elsewhere. Regarding equatorial interleaving, we note that linear double diffusively-driven instability is absent in a neighbourhood of observed mean gradients. Postulating unstable gradients around 3 times larger, we obtain large-amplitude interleaving structures only by employing fingering diffusivities at the upper limit of observational estimates (10^{-4} m^2 s^{-1}) and a low value for the diffusivity in the opposing, S-stable (diffusive) double-diffusive regime (10^{-5} m^2 s^{-1}). In realistic double-diffusively driven cases we obtain effective diffusivities, κ_{eff} between 20 and 400 m^2 s^{-1}.

A further issue is the length of the equilibrated intrusions. Modelled intrusion lengths in realistic double-diffusive cases are between 10 and 40 km, somewhat less than observed. Although we can only perform a limited number of nonlinear simulations, we can estimate this length from the linear solution. The linear solutions have Gaussian y-dependence with a length scale L given approximately by $L^2 = 2N/(\beta m)$ and harmonic z-dependence. Assuming that equilibration, at amplitude a, occurs without strong changes to these functional forms, the intrusion length l at equilibrium, measured as the horizontal displacement of the central salinity contour (see figure 1), can easily be shown to be the solution of the equation

$$\exp\left(-\frac{\beta m}{8N}l^2\right) = \frac{aml\overline{S}_y}{2\overline{S}_z}. \tag{12}$$

For the parameters of run OBS1 and OBS3 (12) gives $l = 7$ km at $a = 3$ and $l = 30$ km at $a = 13$, somewhat underestimating the calculated values. The maximum value of l predicted by (12) throughout the surface corresponding to figure 7 at $a = 13$ is $l \approx 80$ km while the maximum value in the entire range $0.001 < \overline{S}_z < 0.01$ psu m^{-1}, $-10^{-5} < \overline{S}_y < -10^{-6}$ psu m^{-1}, $10^{-5} < N^2 < 2.5 \times 10^{-4}$ s^{-1} is 55 km for $a = 3$ and 95 km for the extreme value $a = 13$. Thus intrusion lengths up to around 100 km may be plausible within this parameter range, according to this estimate. Increases in Prandtl number σ may also increase l via changes in m, as seen in Section 5(b).

It is of interest to compare modelled cross-equatorial diffusivities κ_{eff} with estimates obtained from simple scaling. An approximate balance of along-layer advection and vertical diffusion suggests the estimate

$$v\overline{S}_y \approx AS'/H^2, \tag{13}$$

where subscripts denote derivatives and S' is the salinity perturbation. This gives an estimate for the lateral flux of

$$vS' = -\kappa_{\text{eff}}\overline{S}_y \approx \frac{AS'^2}{H^2\overline{S}_y}, \tag{14}$$

hence, by our definition of a,

$$\kappa_{\text{eff}} \approx Aa^2\frac{\overline{S}_z^2}{\overline{S}_y^2}, \tag{15}$$

cf Joyce (1977) who effectively assumed $a = 1$, whereas we obtain values for a between 3 and 13. For the standard run (15) gives a value of 160 m^2 s^{-1} compared to our calculated value of 110 m^2 s^{-1}, while for the more realistic OBS1 (15) gives a value of 30 m^2 s^{-1} compared with a calculated value of 19 m^2 s^{-1}. The Joyce scaling (15 with a constant) implies quadratic dependence on mean gradients, while we obtain a dependence closer to linear from runs SZ and SY, however, taking the change in a into account we find that for

13

runs S, SY, SZ and OBS1, the estimates are consistently around 50 % too large. The scaling relation (15) underestimates sensitivity to A and fails to take account of some important parameters, but with a set to a constant value of $a = 3$ from our standard run, the estimate remains within an order of magnitude of the calculated result in all cases considered.

Finally, by way of comparison, we give a single example of inertial instability driving intrusive layers up to 190 km in length giving an effective diffusivity four times larger than any realistic double-diffusive simulation. Richards and Edwards (2003) give further evidence for the potential of inertial instability to produce interleaving, and propose a parameterization for the effective lateral diffusion coefficient.

Along-layer density ratios R_l can be calculated for both double-diffusive and inertial cases. As noted by McDougall (1985) values in double-diffusive cases are expected to be close to 0.9. In two dimensions the calculation is complicated by the fact that layer slopes vary with latitude and between temperature and salinity perturbations. The inertially driven linear solutions of Edwards and Richards (1999) feature a strong negative peak of layer slope at the centre of the disturbance where R_l approaches R_ρ, although typical values of R_l are between 0.8 and 2.2 for the parameters used in that paper. For our nonlinear, double-diffusively driven solutions R_l lies between 0.85 and 0.95 in almost all cases, the nonlinear contribution to R_l being very small. For the single inertially driven case a value of 1.03 is obtained at the centre of the disturbance at finite amplitude. When solutions reach very large amplitude, strong dislocation of T and S maxima and strong curvature can give locally more extreme values of R_l.

A pertinent question concerning the driving mechanism for instability is whether much larger amplitude double-diffusive intrusions are precluded by our simple form of diffusivity. A higher-order turbulence closure might permit a vertical localisation of diffusivity onto the interfaces, thus allowing relatively strong diffusive interfacial fluxes to drive intrusions with low interior mixing and thus relatively undisturbed water-mass properties. Double-diffusively driven intrusions of this type can be readily produced at laboratory scale, however, it is not immediately apparent why our 1st order turbulence closure should be inadequate in the present context since time-dependence, advection and non-local effects on the sub-grid scale fluxes would be expected to be small. In a more general sense, proving the inability of double diffusion to reproduce observed intrusion amplitudes by modelling results alone would be almost impossible. After a fairly thorough investigation, however, we find that large amplitude double-diffusive states can only be achieved using mean gradients several times greater than observed and microscale diffusivities at the limit of observational estimates. Even so, intrusion lengths remain rather small. Inertial instability, by contrast, readily produces large intrusions (Richards and Edwards 2003). Richards and Banks (2002) find that the instantaneous flow (as opposed to the time mean) is unstable to inertial instability a significant amount of the time. A thorough examination of inertial instability with double-diffusively driven fluxes within the thermocline at the equator will be the subject of subsequent papers but here we note that even if double-diffusive effects are not the primary mechanism for the formation of the observed intrusions, double diffusion may well play a role at finite amplitude, influencing both the vertical and horizontal fluxes of tracers.

REFERENCES

Balmforth, N. J., S. G. Llewellyn-Smith and W. R. Young. 1998. Dynamics of interfaces and layers in a stratified turbulent fluid. J. Fluid Mech., *355,* 329–358.

Edwards, N. R. and K. J. Richards. 1999. Linear double-diffusive-inertial interleaving at

14

the equator. J. Fluid Mech., *395,* 295-319.

Hua, B. L., D. W. Moore and S. Le Gentil. 1997. Inertial nonlinear equilibration of equatorial flows. J. Fluid Mech., *331,* 345-371.

Joyce, T. M. 1977. A note on the lateral mixing of water masses. J. Phys. Oceanog., *7,* 626-629.

Krishnamurti, R. 2003. Double-diffusive transport in laboratory thermohaline staircases. J. Fluid Mech., *483,* 287-314.

Kunze, E. 1987. Limits on growing, finite-length salt fingers, a Richardson number constraint. J. Mar. Res., *45,* 533-556.

Kunze, E. 1994. A proposed flux constraint for salt fingers in shear. J. Mar. Res., *52,* 999-1016.

Lee, J. H. and K. J. Richards. 2004. The three-dimensional structure of interleaving layers in the western equatorial Pacific Ocean. Submitted to Geophys. Res. Lett.

McDougall, T. J. 1985. Double-diffusive interleaving. Parts I and II. *J. Phys. Oceanog.,* **15,** 1532-1555.

McPhaden, M. J. 1985. Fine-structure variability observed in CTD measurements from the central equatorial Pacific. J. Geophys. Res., *90,* 11726-11740.

Merryfield, W. J. 2000. Origin of thermohaline staircases. J. Phys. Oceanog., *30,* 1046-1068.

Posmentier, E. S. 1977. Generation of salinity finestructure by vertical diffusion. J. Phys. Oceanog., *7,* 298-300.

Radko, T. 2003. A mechanism for layer formation in a double-diffusive fluid. J. Fluid Mech., *in press.*

Rayleigh, Lord 1916. On the dynamics of revolving fluids. Proc. Roy. Soc. London, *A93,* 447-453.

Richards, K. J. 1991. Double-diffusive interleaving at the equator. J. Phys. Oceanog., *21,* 933-938.

Richards, K. J. and H. Banks. 2002. Characteristics of interleaving in the western equatorial Pacific. J. Geophys. Res., *107(C12),* 3231, doi:10.1029/2001JC000971.

Richards, K. J. and N. R. Edwards. 2003. Lateral mixing in the equatorial Pacific: the importance of inertial instability. Geophys. Res. Letters, *30(17),* art. no. 1888.

Richards, K. J. and R. T. Pollard. 1991. Structure of the upper ocean in the western equatorial Pacific. Nature, *350,* 48.

Ruddick, B. R. and D. Hebert. 1988. The mixing of meddy 'sharon', in Small-scale turbulence and mixing in the ocean, edited by J. Nihoul and B. Jamart, pp 249-261. Elsevier, Amsterdam.

Schmitt, R. W. 1981. Form of the temperature-salinity relationship in the central water - evidence for double-diffusie mixing. J. Phys. Oceanog., *11,* 1015-1026.

Stern, M. E. 1967. Lateral mixing of water masses. Deep-Sea Res., *14,* 747-753.

Stern, M. E. 1975. Ocean Circulation Physics, Academic Press, New York, 246 pp.

Toole, J. M. 1981. Anomalous characteristics of equatorial thermocline finestructure. J. Phys. Oceanog., *11,* 871-876.

Walsh, D. and E. Carmack. 2003. The nested structure of Arctic thermohaline intrusions. Ocean Modelling., *5.,* 267-289.

Walsh, D. and B. Ruddick. 1995. Double-diffusively driven intrusions: the influence of non-constant diffusivities. J. Phys. Oceanog., *25,* 348-358.

Walsh, D. and B. Ruddick. 1995b. An investigation of Kunze's salt finger flux laws - are they stable? in Double-diffusive convection, Geophys. Monogr. No. 94, Amer. Geophys. Union, 334 pp.

Walsh, D. and B. Ruddick. 1998. Nonlinear equilibration of thermohaline intrusions. J. Phys. Oceanog., *28,* 1043-1070.

Walsh, D. and B. Ruddick. 2000. Double-diffusive interleaving in the presence of turbulence - the effect of a nonconstant flux ratio. J. Phys. Oceanog., *30,* 2231-2245.
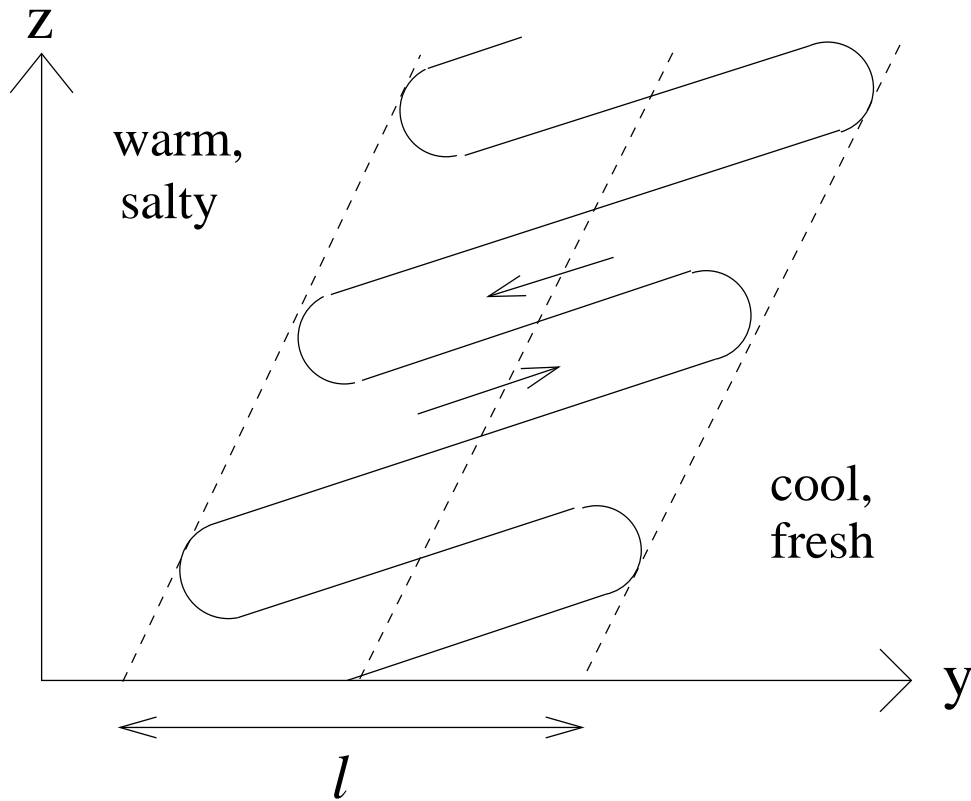
List of Figures

Figure 1: Schematic representation of interleaving structure showing background isohalines; dashed, and an isohaline in the fully developed, large amplitude state; continuous. Intrusive layers containing warm, salty water rise across isopycnals as indicated by the arrows. The instability mechanism is explained, in terms of vorticity dynamics, by Edwards and Richards (1999). Intrusion length l is defined here as the maximum lateral displacement of a central contour as indicated.
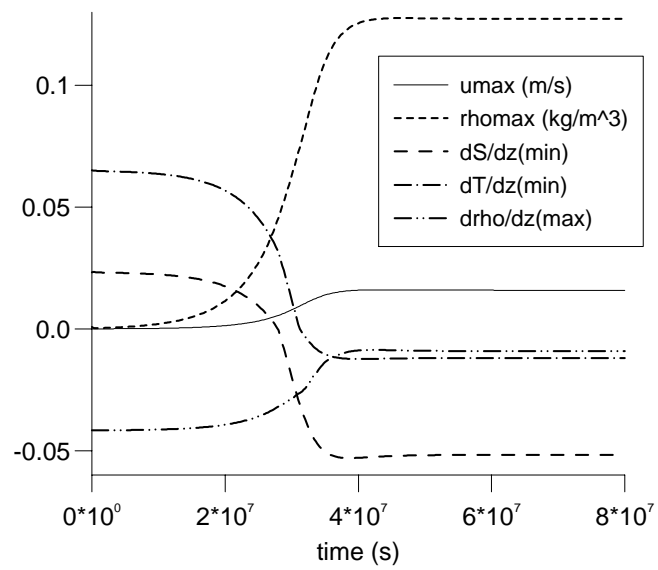
Figure 2: Maximum zonal velocity and density perturbation along with the minimum values of vertical gradients of temperature and salinity and the maximum value of the vertical density gradient. 10^7s$\approx$ 100 days. Units are psu/m for $\partial S/\partial z$, K/m for $\partial T/\partial z$ and kg/m^4 for $\partial\rho/\partial z$.
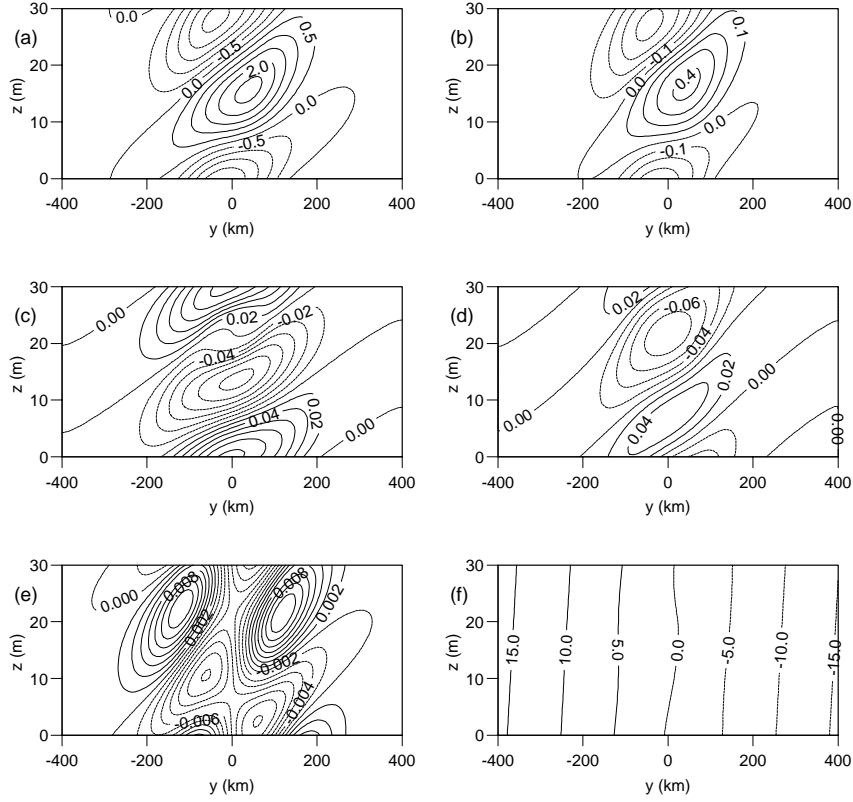
Figure 3: Perturbation fields of temperature (a), salinity (b), density (c), streamfunction (d), zonal velocity (e) and total salinity field (f) for the final state of run S. Extreme values are ±2.7 K (a), ±0.44 psu (b), ±0.13 kg m^{-3} (c), -0.095, +0.059, m^2 s^{-1} (d), -0.014, +0.016 m s^{-1} (e), -16, +17 psu (f). Note that the large and uniform background salinity gradients lead to unrealistically large variations in salinity.

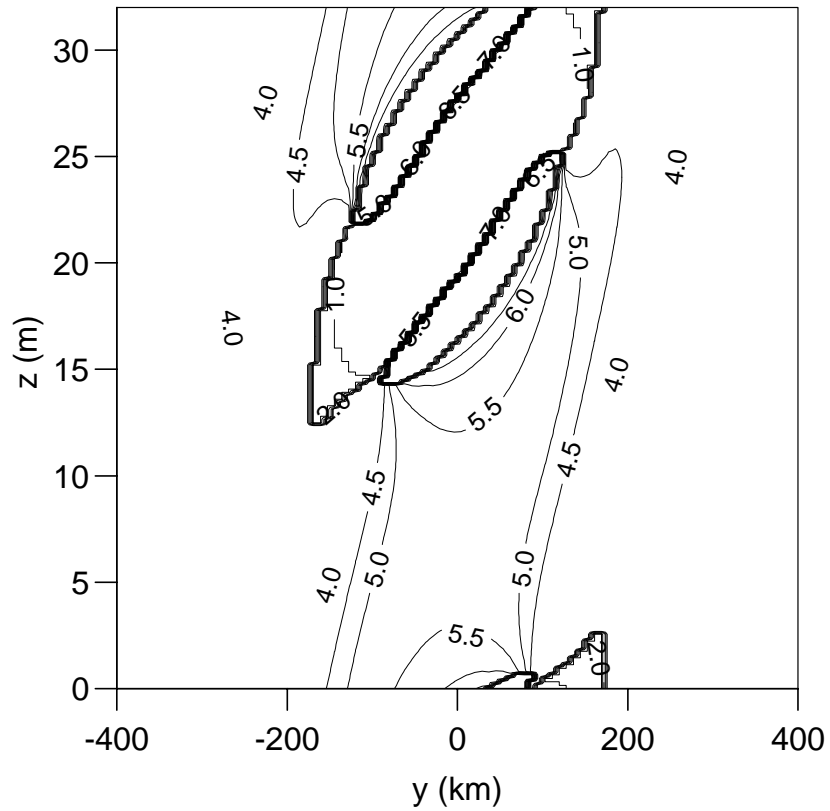Figure 4: Vertical diffusivity of salinity in the final steady state of run D-2 in units of 10^{-5} m^2 s^{-1}. The centre of the fingering region is at around $z = 7.5$. The diffusivity is equal to 16×10^{-6} m^2 s^{-1} in the S-stable region centred at $z = 22.5$ and is equal to 10^{-4} m^2 s^{-1} in the convective regions above and below.

Figure 5: Maximum density perturbation, average advective northward heat flux at the equator and maximum vertical density gradient for a run with no dissipation of temperature and salinity in stable regions apart from double diffusion, $\kappa_s = r = \kappa_y = 0$. 10^7s≈ 100 days.
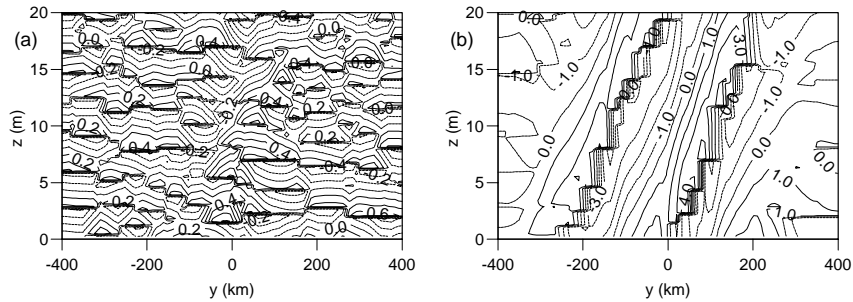
Figure 6: Temperature perturbation for a run with flux ratio a decreasing function of density ratio and with turbulent diffusivity κ_s set to zero (a) after development of staircase structure at $t = 4 \times 10^6$ s, (b) after equilibration of interleaving structure at $t = 1.6 \times 10^7$ s. A single convective layer remains, bounded by steppy fingering interfaces.

22
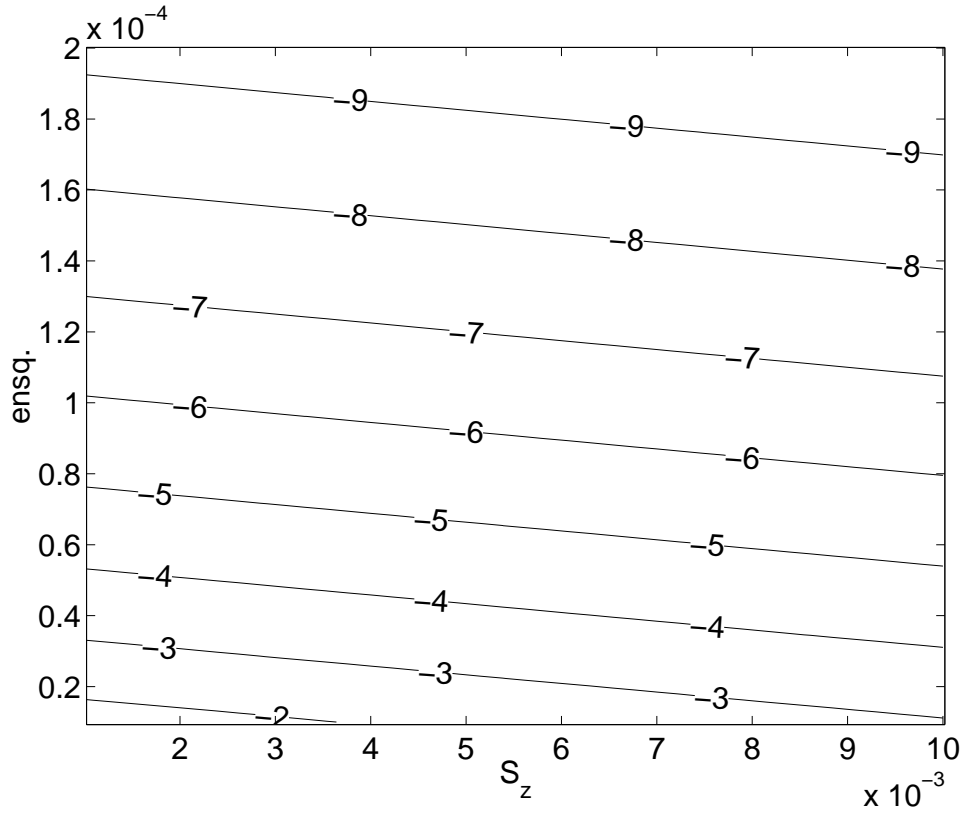
Figure 7: The value of $\overline{S}_y$, in 10^{-6} psu m^{-1} at which the linear growth rate equals 10^{-7} s^{-1} as a function of N^2, in s^{-1}, and $\overline{S}_z$, in psu m^{-1}.
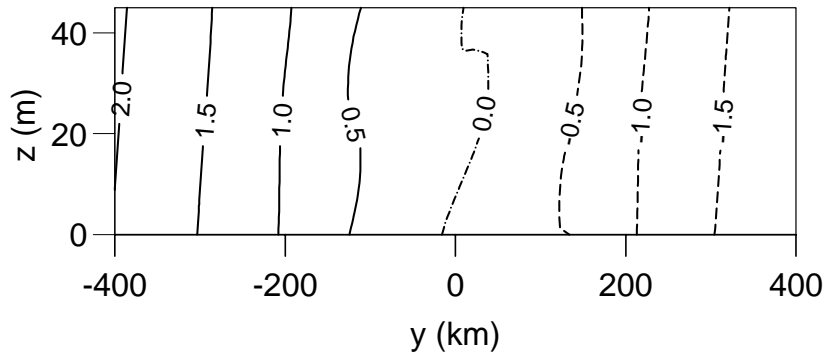
Figure 8: Contours of total salinity for a double-diffusively driven run with realistic parameters chosen to give optimally large amplitude interleaving, parameters for the run, labelled OBS3, are given in Table 2.
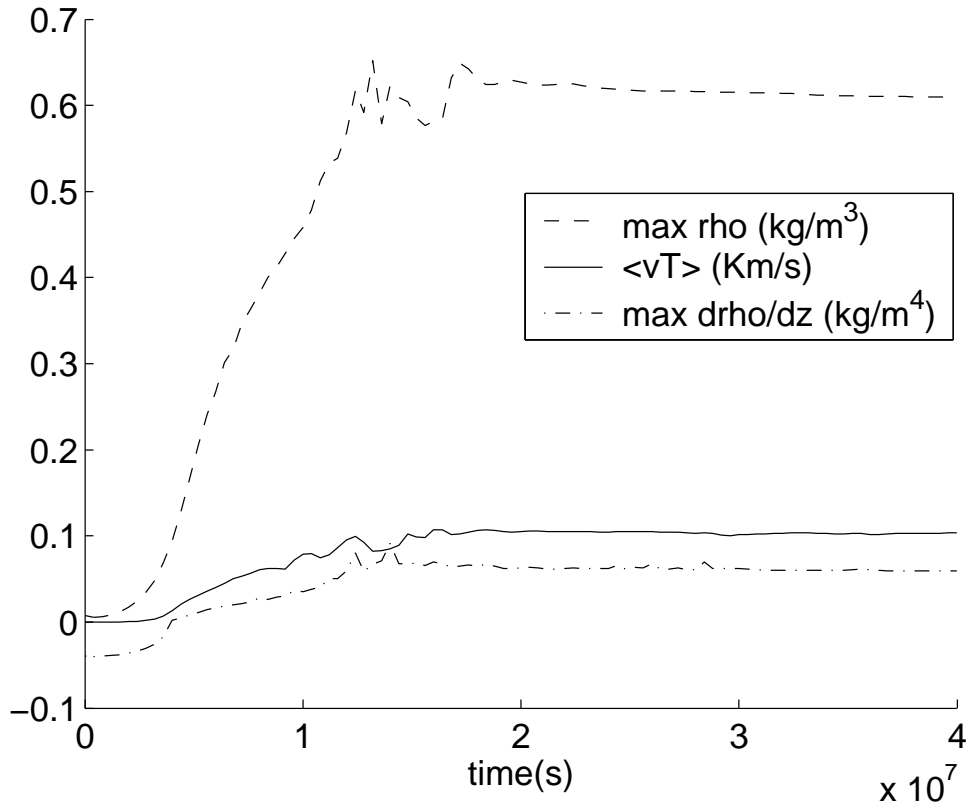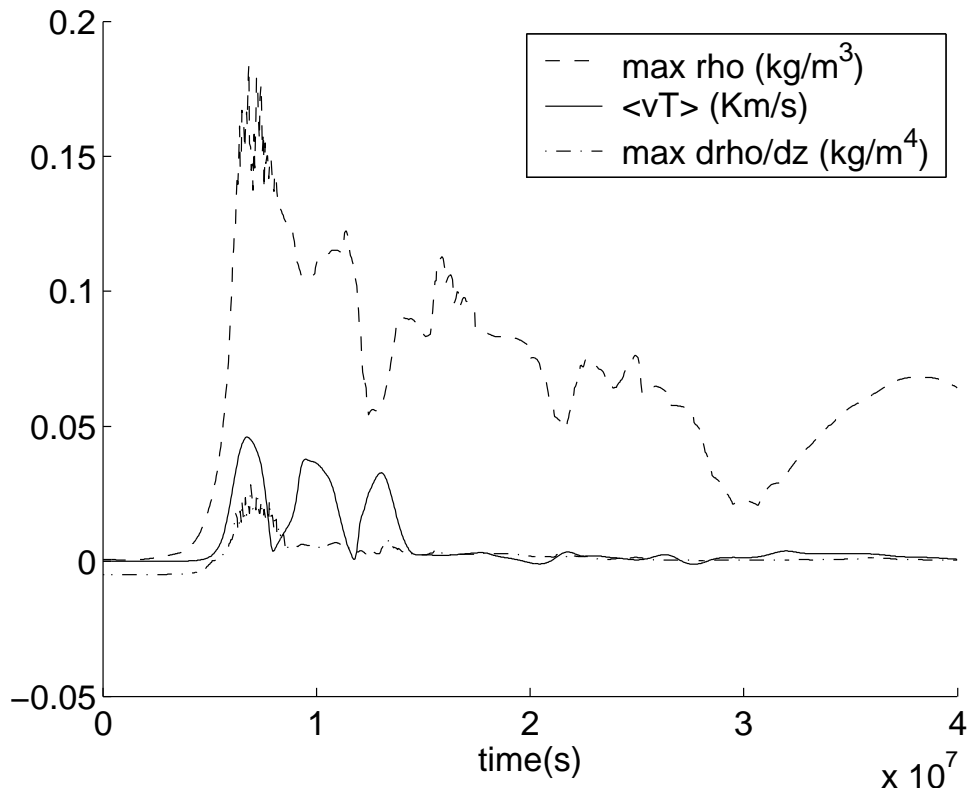
Figure 9: Maximum density perturbation, average advective northward heat flux at the equator and maximum vertical density gradient for an inertially unstable case.
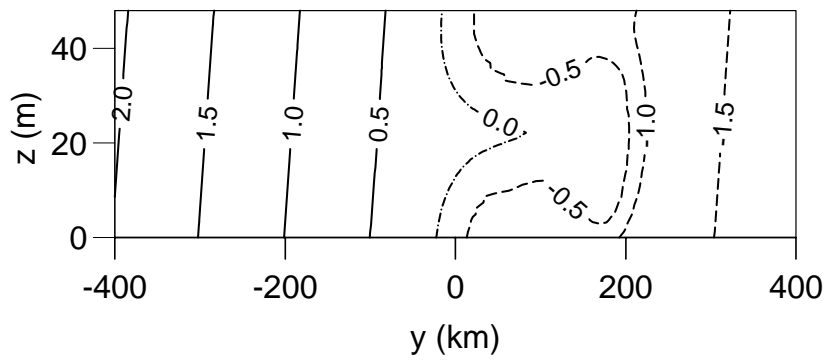
Figure 10: Contours of total salinity for an inertially unstable basic state after about 60 days integration, close to the time of peak amplitude of the disturbance.

Table 1: Values of constants used in main run.

| parameter	value	interpretation
β	2.289×10^{-11} m^{-1}s^{-1}	gradient of Coriolis parameter
g	9.78 ms^{-2}	gravitational acceleration
ρ_0	1020 kg m^{-3}	reference density
ν_y	300 m^{2}s^{-1}	meridional viscosity
ν_z	3×10^{-5} m^{2}s^{-1}	vertical viscosity
r	10^{-7} s^{-1}	Rayleigh drag
δ	$0.78\rho_0$ psu^{-1}	salinity contraction coefficient
α	$0.17\rho_0$ K^{-1}	thermal expansion coefficient
A_F	3×10^{-5} m^{2}s^{-1}	salinity diffusivity (fingers)
γ_F	0.5	flux ratio (fingers)
A_D	0.6×10^{-5} m^{2}s^{-1}	salinity diffusivity (diffusive)
γ_D	5	flux ratio (diffusive)
κ_s	10^{-5} m^{2}s^{-1}	turbulent viscosity
κ_u	10^{-4} m^{2}s^{-1}	convective viscosity
H	30 m	domain height
L	800 km	domain width
N	0.02 s^{-1}	buoyancy frequency
$\partial S / \partial y$	-4×10^{-5} psu m^{-1}	meridional salinity gradient
$\partial S / \partial z$	0.03 psu m^{-1}	vertical salinity gradient

Table 2: Parameters for the numerical runs. Diffusivities and viscosities are in units of 10^{-5} m^2 s^{-1}, Rayleigh drag r is given in units of 10^{-7} s^{-1}, the initial salinity gradients $\overline{S}_y$ and $\overline{S}_z$ are given in units of 10^{-5} psu m^{-1} and psu m^{-1} respectively. For runs with variable diffusivity, maximum and minimum values are given, see Table 4 for details. For runs with variable diffusivity, $\sigma = (A + \kappa_s)/\nu$. Run II has an imposed mean shear $\overline{u}_y = 4 \times 10^{-6}$ s^{-1}.

run	H (m)	A_F	A_D	γ_D	κ_s	κ_u	r	$\overline{S}_y$	$\overline{S}_z$	σ	comments
S	30	3	0.6	5	1	10	1	-4	0.03	1	standard
XPF	300	3	0.6	5	1	10	0	-4	0.03	1	no pert'n flux b.c.
D	30	3	0.6	5	1	10	1	-4	0.03	1	linear advection
A	30	3	3	0.6	1	1	1	-4	0.03	1	no regime changes
AH	30	3	3	0.6	1	1	1	-4	0.03	1	as A, hydrostatic
WB	30	3	0	1	1	10	1	-4	0.03	1	weak braking
SZ	30	3	0.6	5	1	10	1	-4	0.06	1	$2\times\partial S/\partial z$
SY	25	3	0.6	5	1	10	1	-8	0.03	1	$2\times\partial S/\partial y$
2S	34.5	3	0.6	5	1	10	1	-4	0.03	2	$2\times\sigma$
D2	34.5	6	0.6	5	1	10	1	-4	0.03	1	$2\times A_F$
D4	44	12	0.6	5	1	10	1	-4	0.03	1	$4\times A_F$
D+2	32	1.5<3	0.6	5	1	10	0	-4	0.03	1	$A_F(R_\rho)$
D-2	32	3<6	0.6	5	1	10	0	-4	0.03	1	$A_F(R_\rho)$
D+5	32	0.6<3	0.6	5	1	10	1	-4	0.03	1	$A_F(R_\rho)$
D-5	32	3<15	0.6	5	1	10	0	-4	0.03	1	$A_F(R_\rho)$
K/2	26	3	0.6	5	0.5	10	1	-4	0.03	1	$0.5\times\kappa_s$
K0	20	3	0.6	5	0	10	1	-4	0.03	1	$\kappa_s = 0$
T0	20	3	0.6	5	0	10	0	-4	0.03	1	$\kappa_s = r = \kappa_y = 0$
GR	20	3	0.6	5	0	10	1	-4	0.03	1	$\gamma_F(R_\rho), \kappa_s = 0$
OBS1	20	1	0.2	5	0.1	10	0	-0.5	0.002	1	$N_0 = 0.007$ s^{-1}
OBS2	45	10	2	5	0.1	10	0	-0.5	0.002	1	$N_0 = 0.007$ s^{-1}
OBS3	45	10	0.2	5	0.1	10	0	-0.5	0.002	1	$N_0 = 0.007$ s^{-1}
II	48	1	0.2	5	0.2	10	0	-0.5	0.002	1	$N_0 = 0.007$ s^{-1}

Table 3: Results at steady state, or maximum values in cases marked *. Note that in all cases except OBS1, OBS2, OBS3 and II, the driving thermohaline gradients are unrealistically large and it is the relative amplitude of solutions which should be considered significant. The amplitude a for run XPF is calculated for the central layer in the domain.

run	$\overline{vT}$	$\max(\rho')$	intrusion	κ_{eff}	a
	K m s^{-1}	kg m^{-3}	length (km)	m^2 s^{-1}	
S	0.0196	0.127	20	110	3.1
XPF	0.0251	0.195	29	140	6.4
D	0.0203	0.131	19	110	2.8
A	0.219	0.294	81	1200	14
AH	0.261*	0.629*	95*	1400*	21*
WB	0.086	0.202	49	469	8.4
SZ	0.0465	0.195	30	250	2.3
SY	0.0261	0.196	15	70	5.2
2S	0.0214	0.148	24	120	3.3
D2	0.0626	0.3	32	340	4.5
D4	0.247	0.677	64	1300	8.3
D+2	0.0120	0.114	20	65	2.9
D-2	0.0392	0.231	29	210	5.3
D+5	0.00455	0.0568	3	25	0
D-5	0.0563	0.280	30	310	8.2
K/2	0.0273	0.214	22	150	3.9
K0	0.0367	0.403	13	200	3.3
T0	0.103	0.61	26	561	13
GR	0.0737	0.532	16	421	4.6
OBS1	4.26×10^{-4}	0.0206	10	19	4.4
OBS2	3.71×10^{-3}	0.102	17	162	6.3
OBS3	9.66×10^{-3}	0.0981	43	421	13
II	0.046*	0.184*	190*	2000*	50

Table 4: Parameters for runs with variable diffusvity. Diffusivities are in units of 10^{-5} m^{2}s^{-1}.

run	R_1	R_2	A_1	A_2
D+2	1.5	2.5	1.5	3
D-2	1.5	2.5	6	3
D+5	1.5	2.5	0.6	3
D-5	1.5	2.5	15	3